Biophysical journal, Volume 99

Supporting Material

Excitation dynamics in phycoerythrin 545: modeling of steady-state spectra and transient absorption with modified Redfield theory

Vladimir I. Novoderezhkin, Alexander B. Doust, Carles Curutchet, Gregory D. Scholes, and Rienk van Grondelle

SUPPORTING MATERIAL

This Supporting Material includes 8 sections containing:

- expressions needed to calculate the linear spectra;
- parameters of the exciton-phonon spectral density for PE545
- expressions for fluorescence excitation anisotropy;
- expressions for transient absorption
- site energies for the working and alternative models
- illustration of the TA spectra predicted by models E68 and E17;
- comparison of the working model E and model E47;
- comparison of the working model E and model E42.

Linear spectra

The absorption (OD), circular dichroism (CD), and steady-state non-selective fluorescence (FL) spectra are given by (Mukamel, 1995; Zhang et al., 1998; Novoderezhkin et al., 2005):

$$\begin{aligned}
&\mathrm{OD}(\omega) = \omega\sum_k \mathbf{d}_{kg}^2\ \mathrm{Re}\int_0^\infty dt\exp\left\{ i(\omega-\omega_{kg})t - \sum_n (c_n^k)^4 g(t) - \frac{t}{2\tau_k}\right\};\\
&\mathrm{CD}(\omega) = \omega\sum_k \mathbf{m}_{kg}\mathbf{d}_{kg}\ \mathrm{Re}\int_0^\infty dt\exp\left\{ i(\omega-\omega_{kg})t - \sum_n (c_n^k)^4 g(t) - \frac{t}{2\tau_k}\right\};\\
&\mathrm{FL}(\omega) = \omega\sum_k P_k\mathbf{d}_{kg}^2\ \mathrm{Re}\int_0^\infty dt\exp\left\{ i(\omega-\omega_{kg})t + 2it\sum_n (c_n^k)^4\lambda - \sum_n (c_n^k)^4 g^*(t) - \frac{t}{2\tau_k}\right\};\\
&\mathbf{d}_{kg} = \sum_n c_n^k\mathbf{d}_n \quad ; \quad \mathbf{m}_{kg} = \sum_n c_n^k[\mathbf{R}_n\mathbf{d}_n] \quad ; \quad \frac{1}{\tau_k} = -\sum_{k'\neq k} R_{k'k'kk}
\end{aligned} \tag{S1}$$

where P_k denote the steady-state population of the k-th state, ω_{kg} is the energy of transition from the ground to k-th exciton state, $\mathbf{d}_{kg}$ is transition dipole and $\mathbf{m}_{kg}$ is rotational moment of the k-th exciton state (expressed through a transition dipole $\mathbf{d}_n$ and radius –vector $\mathbf{R}_n$ of the n-th molecule listed in Table 1). The wavefunction amplitudes c_n^k give the participation of the n-th pigment in the k-th exciton state. The phonon-induced lineshape is given by function g(t). The relaxation-induced broadening is given by the inverse lifetime of the exciton state τ_k (the latter is expressed as the sum of transfer rates $R_{k'k'kk}$. from k-th to other (k'≠k) states). The transfer rates are given by the modified Redfield tensor as described elsewhere (Zhang et al., 1998). Notice that Eqs. S1 give homogeneous line shapes, i.e. including the relaxation-induced and phonon-induced broadening. In the presence of static disorder (for example site inhomogeneity) the homogeneous spectra should be averaged over a random distribution of the site energies that will perturb the energies ω_{kg} and eigenfunctions c_n^k of the exciton states.

The line-broadening function g(t) and reorganization energy in the site representation λ are:

$$\begin{aligned}
&g(t) = -\int_{-\infty}^{\infty}\frac{d\omega}{2\pi\omega^2}C(\omega)\left[\coth\frac{\omega}{2k_BT}(\cos\omega t - 1) - i(\sin\omega t - \omega t)\right]\\
&\lambda = -\lim_{t\to\infty}\frac{d}{dt}\mathrm{Im}\{g(t)\} = \int_{-\infty}^{\infty}\frac{d\omega}{2\pi\omega}C(\omega)
\end{aligned} \tag{S2}$$

where $C(\omega)$ is the spectral density of exciton-phonon coupling, k_B is the Boltzmann constant, T is the temperature. Notice that the lineshape function g(t) and the reorganization energy λ in the exciton representation (as they appear in Eq. S1) are smaller than in the site representation being multiplied by the participation ratio $\sum_n (c_n^k)^4$ (which is equal to the inverse delocalization length of individual exciton states). To construct the spectral density profile we use the sum of M overdamped Brownian oscillators and J resonance contributions due to high-frequency modes:

$$C(\omega) = \sum_{m=1}^{M} 2\lambda_{0m} \frac{\omega\gamma_{0m}}{\omega^2 + \gamma_{0m}^2} + \sum_{j=1}^{J} 2\lambda_j \omega_j^2 \frac{\omega\gamma_j}{(\omega_j^2 - \omega^2)^2 + \omega^2\gamma_j^2} \quad ; \quad \lambda_j = S_j\omega_j$$
$$\lambda = \int_{-\infty}^{\infty} \frac{d\omega}{2\pi\omega} C(\omega) = \sum_{m=1}^{M} \lambda_{0m} + \sum_{j=1}^{J} \lambda_j \qquad \text{(S3)}$$

where λ_{0m} and γ_{0m} denote coupling and characteristic frequency of m-th Brownian oscillator, ω_j, λ_j and γ_j are frequency, coupling and damping constant for the j-th vibrational mode, S_j is the Huang-Rhys factor of the j-th vibrational mode.

Spectral density for PE545 complex

For modeling of the PE545 complex the spectral density (Eq S3) is constructed as a sum of two overdamped Brownian oscillators (characteristic frequencies γ_{01}=30 cm^{-1}, γ_{02}=90 cm^{-1} and couplings λ_{01}=40 cm^{-1}, λ_{02}=70 cm^{-1}) and 14 underdamped vibrations with frequencies ω_j and Huang-Rhys factors S_j listed in the Table S1. Brownian oscillators describe the coupling of excitations to low-frequency phonons (collective nuclear modes of the pigment-protein matrix), whereas vibrations correspond to high-frequency intramolecular modes of phycobilins. The high-frequency vibrations have a total Huang-Rhys factor of S=0.62 and determine a most part of reorganization shift (i.e. 523 cm^{-1} of the total shift of 633 cm^{-1}). These parameters of spectral density are taken according to earlier suggestion (Doust et al.,2004) and further adjusted from a fit of the 77K and room temperature fluorescence spectra. The damping constants γ_j are taken to be 20 cm^{-1} for all vibrations (the exact value is not known, on the other hand its variation does not influence the calculated spectra that are strongly inhomogeneously broadened).

Table S1. Frequencies ω_j (cm^{-1}) and Huang-Rhys factors S_j for nuclear modes j=1-14 ($\sum S_j$=0.62). Data was taken from the experiment (Doust et al., 2004) and further adjusted from the fit of fluorescence spectra.

ω_j	S_j	ω_j	S_j
207	0.0013	813	0.0578
244	0.0072	938	0.0313
312	0.0450	1111	0.0578
372	0.0578	1450	0.1013
438	0.0450	1520	0.0265
514	0.0924	1790	0.0072
718	0.0761	2090	0.0113

Fluorescence excitation anisotropy

Fluorescence excitation spectrum (FLE) is:

$$\mathrm{FLE}(\omega) = \sum_{k} \mathrm{OD}_k(\omega, \mathbf{d}_{kg}^{ex}) \sum_{k'} \mathrm{FL}_{k'}(\omega_{pr}, \mathbf{d}_{k'g}^{pr}) \quad , \tag{S4}$$

where OD_k and $\mathrm{FL}_{k'}$ are exciton components of the OD and FL spectra (given by Eq S1), dependent on excitation and probe frequencies (ω and ω_{pr}) and projection of the transition dipole moments $\mathbf{d}_{kg}$ on the polarization vectors of the excitation and probe. (In Eq S1 these projections have been replaced by the absolute values of the dipoles $\mathbf{d}_{kg}$ after averaging over random orientations of the antenna). Fluorescence excitation anisotropy (EA) is:

$$\mathrm{r}(\omega) = \frac{\mathrm{FLE}_{II}(\omega) - \mathrm{FLE}_{\perp}(\omega)}{\mathrm{FLE}_{II}(\omega) + 2 \cdot \mathrm{FLE}_{\perp}(\omega)} \quad , \tag{S5}$$

where subscripts FLE_{II} and $\mathrm{FLE}_{\perp}$ denote FLE spectra measured with parallel and perpendicular polarization of the probe with respect to excitation. The FLE_{II} and $\mathrm{FLE}_{\perp}$ values should be averaged over disorder as well as over all possible orientations of the molecular aggregate with respect to the polarization vectors. In the orientational averaging we use the rules (Novoderezhkin et al., 2003):

$$\begin{aligned} \left\langle \mathbf{d}_{kg}^{ex}\mathbf{d}_{kg}^{ex}\mathbf{d}_{k'g}^{pr}\mathbf{d}_{k'g}^{pr} \right\rangle_{II-\perp} &= \tfrac{1}{15}[-\mathbf{d}_{kg}^2\mathbf{d}_{k'g}^2 + 3(\mathbf{d}_{kg}\mathbf{d}_{k'g})^2] \\ \left\langle \mathbf{d}_{kg}^{ex}\mathbf{d}_{kg}^{ex}\mathbf{d}_{k'g}^{pr}\mathbf{d}_{k'g}^{pr} \right\rangle_{II+2\perp} &= \tfrac{1}{3}\mathbf{d}_{kg}^2\mathbf{d}_{k'g}^2 \end{aligned} \tag{S6}$$

Using Eqs S4-S6 we obtain:

$$\mathrm{r}(\omega) = \sum_{k} \mathrm{r}_k(\omega) = 0.1 \cdot \frac{\sum_{k} \mathrm{OD}_k(\omega) \sum_{k'} \mathrm{FL}_{k'}(\omega_{pr}) \cdot \left[6 \cdot \dfrac{(\mathbf{d}_{kg}\mathbf{d}_{k'g})^2}{\mathbf{d}_{kg}^2\mathbf{d}_{k'g}^2} - 2 \right]}{\sum_{k''} \mathrm{OD}_{k''}(\omega) \sum_{k'} \mathrm{FL}_{k'}(\omega_{pr})} \tag{S7}$$

Now (instead of Eq S4) the OD_k and $\mathrm{FL}_{k'}$ are proportional to the squares of the dipoles ($\mathbf{d}_{kg}$ and $\mathbf{d}_{k'g}$) as in Eq S1. The r_k value is the contribution of the k-th level to the anisotropy. This contribution varies between –0.2 (when the absorbing $\mathbf{d}_{kg}$ and emitting $\mathbf{d}_{k'g}$ dipoles are perpendicular) and 0.4 (for parallel $\mathbf{d}_{kg}$ and $\mathbf{d}_{k'g}$).

Transient absorption

The transient absorption (TA) can be expressed as a sum of the photobleaching (PB), stimulated emission (SE), and excited state absorption (ESA). In the doorway-window representation (Mukamel, 1995; Zhang et al., 1998) we get:

$$\mathrm{PB} = -\omega_2\, W_{gg}(\omega_2) \sum_{k'} D_{k'k'}(0,\omega_1)$$
$$\mathrm{SE} = -\omega_2 \sum_{k} W_{kk}(\omega_2)\, D_{kk}(\tau,\omega_1) \qquad \text{(S8)}$$
$$\mathrm{ESA} = \omega_2 \sum_{k} W'_{kk}(\omega_2)\, D_{kk}(\tau,\omega_1)$$

where ω_1 and ω_2 are pump and probe frequencies, τ is the pump-probe delay. For delays larger than the pulse duration the TA kinetics can be calculated in a sequential approximation, i.e. neglecting the pump and probe overlap. Initially, the pump pulse creates a superposition of the excited (one-exciton) states described by the doorway amplitudes $D_{kk}(0,\omega_1)$ together with the hole in the ground state given by $-\sum_k D_{kk}(0,\omega_1)$. The evolution of the excited-state wavepacket due to exciton relaxation/migration during pump-probe delay is given by $D_{kk}(\tau,\omega_1)$. The ground-state hole is time-independent because one-exciton relaxation does not change the number of excitations, i.e. $-\sum_k D_{kk}(\tau,\omega_1)$=const. The absorption of a weak probe is determined by the overlap of the doorway and window wavepackets (Eq S8). The initial doorway amplitude $D_{kk}(0,\omega_1)$, and the window amplitudes $W_{kk}(\omega_2)$, $W'_{kk}(\omega_2)$, and $W_{gg}(\omega_2)$ are given by

$$D_{kk}(0,\omega_1) = \int_{-\infty}^{\infty} dt' \int_{0}^{\infty} dt_1\, \varepsilon_1(t')\,\varepsilon_1(t'-t_1)\, d_{kg}^{e1} d_{kg}^{e1}\, D(\omega_{kg},\omega_1,t_1) + \text{c.c.}$$
$$W_{kk}(\omega_2) = \int_{-\infty}^{\infty} dt \int_{0}^{\infty} dt_3\, \varepsilon_2(t)\,\varepsilon_2(t+t_3)\, d_{kg}^{e2} d_{kg}^{e2}\, W(\omega_{kg},\omega_2,t_3) + \text{c.c.}$$
$$W'_{kk}(\omega_2) = \int_{-\infty}^{\infty} dt \int_{0}^{\infty} dt_3\, \varepsilon_2(t)\,\varepsilon_2(t+t_3) \sum_{q} d_{qk}^{e2} d_{qk}^{e2}\, W'(\omega_{qk},\omega_2,t_3) + \text{c.c.} \qquad \text{(S9)}$$
$$W_{gg}(\omega_2) = \int_{-\infty}^{\infty} dt \int_{0}^{\infty} dt_3\, \varepsilon_2(t)\,\varepsilon_2(t+t_3) \sum_{k} d_{kg}^{e2} d_{kg}^{e2}\, D(\omega_{kg},\omega_2,t_3) + \text{c.c.}$$

where ε_1 and ε_2 are the envelopes of the pump and probe pulses (they are taken to be real). Here we use indices g, k, and q for ground, one- and two-exciton states respectively. Transition dipoles d_{kg} and d_{qk} correspond to $g\rightarrow k$ and $k\rightarrow q$ transitions with the transition frequencies ω_{kg} and ω_{qk}, respectively. These dipoles can be calculated as:

$$\mathbf{d}_{kg} = \sum_{n} c_n^k \mathbf{d}_n$$
$$\mathbf{d}_{qk} = \sum_{m>n} c_{nm}^q (c_n^k \mathbf{d}_m + c_m^k \mathbf{d}_n) + \sum_{n} c_{nn}^q c_n^k \mathbf{d}_{nn} \qquad \text{(S10)}$$

where the wavefunction amplitudes c_n^k give the participation of the n-th pigment in the k-th exciton state, whereas c_{nm}^q give the participation of the excited pair of pigments (n,m) in the q-th two exciton state. Notice that c_{nn}^q corresponds to the contribution of the double-excited state of the n-th pigment in the two-exciton manifold. Transition dipole from the ground to the first excited state of the pigment is $\mathbf{d}_n$, transition dipole from the first to second excited state of the n-th pigment is $\mathbf{d}_{nn}$.

Superscripts e1/e2 in Eq S9 denote projection of the transition dipoles to the polarization vectors of the pump/probe pulses. D, W, and W' are the lineshape functions describing the dephasing during the electronic coherence periods t_1 and t_3. They correspond to ground-state absorption, excited-state emission, and excited-state absorption, respectively. Note that the

window amplitude $W_{gg}(\omega_2)$ depends on the D-function, being determined by the ground-state absorption. In the modified Redfield theory the lineshape functions are (Zhang et al., 1998):

$$\begin{aligned} D(\omega_{kg},\omega_1,t_1) &= \exp\left\{-i(\omega_{kg}-\omega_1)t_1 - g_{kkkk}(t_1)\right\} \\ W(\omega_{kg},\omega_2,t_3) &= \exp\left\{-i(\omega_{kg}-\omega_2)t_3 + 2i\lambda_{kkkk}t_3 - g^{*}_{kkkk}(t_3)\right\} \\ W'(\omega_{qk},\omega_2,t_3) &= \exp\left\{-i(\omega_{qk}-\omega_2)t_3 - g_{kkkk}(t_3) - g_{qqqq}(t_3) + \right. \\ &\qquad \left. + 2g_{kkqq}(t_3) + 2i(\lambda_{kkqq}-\lambda_{kkkk})t_3\right\} \end{aligned} \tag{S11}$$

The line-broadening functions and reorganization energies in the exciton representation (appearing in Eq S11) can be expressed through the site representation values (i.e. g(t) and λ given by Eq S2). If the dynamic disorder (due to coupling to phonons) is described by the uncorrelated diagonal model, then the g-matrices are connected with the g(t)-function by (Novoderezhkin et al., 2004):

$$\begin{aligned} g_{kk'k''k'''}(t) &= \sum_n c_n^k c_n^{k'} c_n^{k''} c_n^{k'''}\, g(t) \\ g_{kkqq}(t) &= \sum_{n<m} (c_{nm}^q c_{n'}^k)^2 (\delta_{nn'}+\delta_{mn'})\, g(t) \\ g_{qqqq}(t) &= \sum_{\substack{n<m \\ n'<m'}} (c_{nm}^q c_{n'm'}^q)^2 (\delta_{nn'}+\delta_{nm'}+\delta_{mn'}+\delta_{mm'})\, g(t) + \sum_n (c_{nn}^q)^4\, g(t) \end{aligned} \tag{S12}$$

and the same equations connect the λ-matrices with the λ value.

The time evolution of the initially created doorway packet is given by

$$\frac{d}{d\tau} D_{kk}(\tau,\omega_1) = -\sum_{k,k'} R_{kkk'k'} D_{k'k'}(\tau,\omega_1) \tag{S13}$$

with the initial conditions given by the first of Eqs S9. The relaxation tensor calculated according to the modified Redfield approach is (Zhang et al., 1998):

$$\begin{aligned} R_{kkk'k'} = -2\,\mathrm{Re}\int_0^\infty dt\, W'(\omega_{kk'},0,t)\{ &\ddot{g}_{kk'k'k}(t) - \{\dot{g}_{k'kk'k'}(t) - \dot{g}_{k'kkk}(t) + 2i\lambda_{k'kk'k'}\}\times \\ &\times\{\dot{g}_{k'k'kk'}(t) - \dot{g}_{kkkk'}(t) + 2i\lambda_{k'k'kk'}\}\} \end{aligned} \tag{S14}$$

Notice that the doorway amplitude $D_{kk}(\tau,\omega_1)$ is equal to the time-dependent population of the k-th exciton state (these populations are not normalized). Remind that the coherences between one-exciton states $D_{k'k}(\tau,\omega_1)$ are not included into the modified Redfield approach. Switching to the site representation we obtain the time-dependent density matrix:

$$\rho_{nm}(\tau,\omega_1) = \sum_{k,k'} c_n^{k'} c_m^k D_{k'k}(\tau,\omega_1) \to \sum_k c_n^k c_m^k D_{kk}(\tau,\omega_1) \tag{S15}$$

Site energies for the working and alternative models

Table S2. The site energies (cm^{-1}) for the pigments from 1 to 8 extracted from the fit of the data. (The values correspond to the electronic transition energies without including a reorganization shift) The energy set for our working model is denoted as E, other sets correspond to alternative models with permutation of some pairs of the site energies (indicated in bold) and with slight adjustment of the other site energies.

Model	$PEB_{50/61C}$	DBV_A	DBV_B	PEB_{82C}	PEB_{158C}	$PEB_{50/61D}$	PEB_{82D}	PEB_{158D}
E	18532	18008	17973	18040	18711	19574	19050	18960
E68	18532	18008	17973	18040	18781	**18809**	19030	**19574**
E67	18532	18008	17973	18040	18781	**18809**	**19574**	19030
E65	18532	18008	17973	18040	**19574**	**18711**	19030	18909
E17	**19050**	18008	17973	18040	18651	19574	**18532**	18050
E47	18641	18043	18030	**19111**	18499	19588	**17909**	18868
E42	18532	**18048**	18013	**17940**	18711	19574	18960	19050

Exploring models with different positions of the $PEB_{50/61}$ levels
(TA spectra predicted by models E68 and E17)

Configurations with different site energies of the $PEB_{50/61}$ dimer are discussed in the main text. Here (Figs. S1 and S2) we show the TA spectra predicted by models E68 and E17.

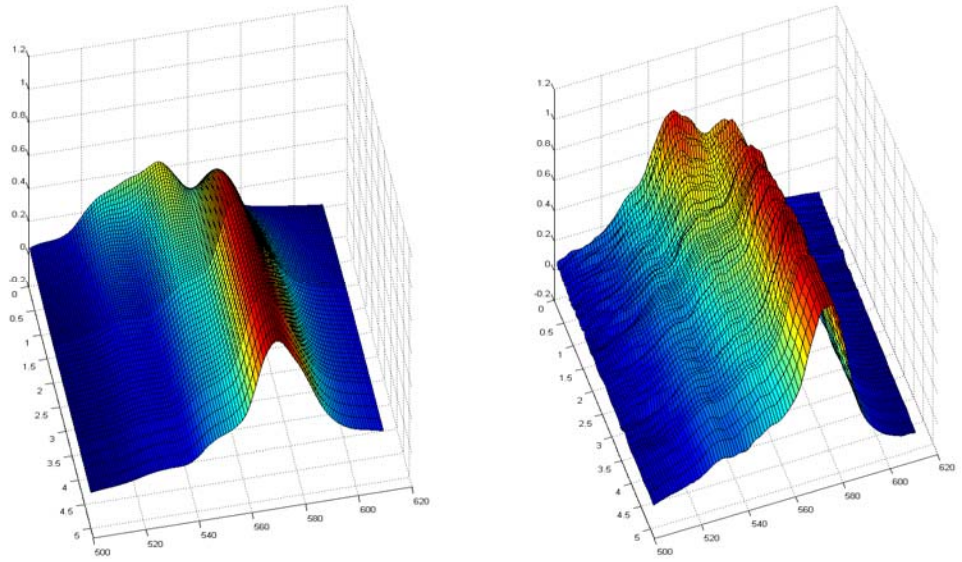

Fig. S1. Comparison of the TA spectra calculated for the E68 model (left) with the measured ones (right). Time delays are from 0 to 5 ps. Note the too slow relaxation of the higher 530 nm band due to the red shift of the upper exciton level of the $PEB_{50/61}$ dimer in the model E68 . In the working model (model E) this band is less pronounced being partially depopulated already during the pump pulse.

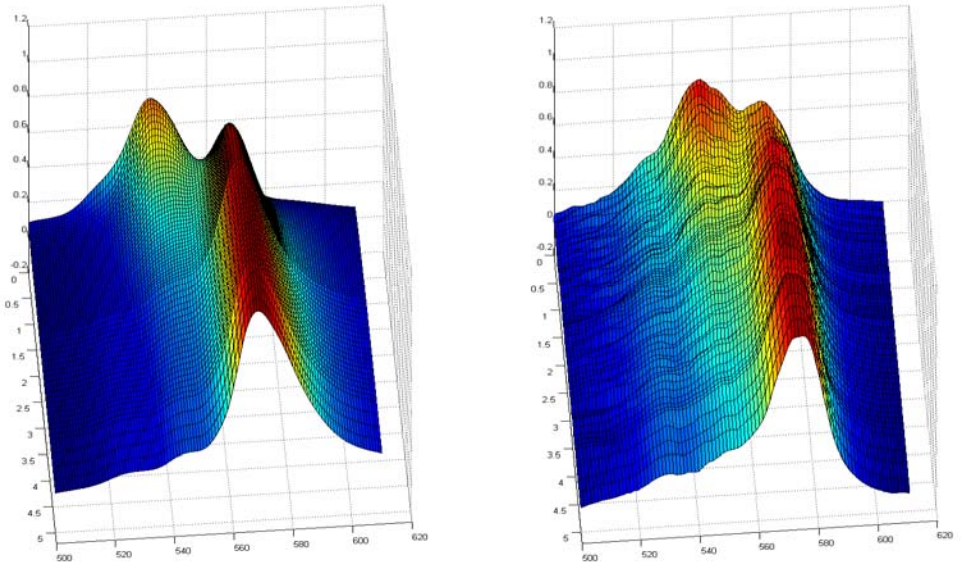

Fig. S2. The same as in Fig. S1, but for the E17 model. Note the very fast depopulation of the 530 nm band and quick formation of the 540 nm bleaching during the pump pulse predicted by the model. This bleaching must be at 547 nm, but after the blue shift of $PEB_{50/61C}$ it has moved to 540 nm.

Permutation of the energies of pseudo-symmetric PEB_{158} and PEB_{82} pairs (comparing model E47 with the working model E)

Fixing the site energies of the 567 nm pool pigments and the heterodimer $PEB_{50/61}$, we can try inversion of the energies of the pseudo-symmetric pair PEB_{158C} and PEB_{158D}. The resulting spectra are not so good as for the working model: the quality of the linear spectra fit is almost the same, but energy transfer is too fast.

On the other hand, the inversion of another pseudo-symmetric pair, i.e. PEB_{82C} and PEB_{82D}, yields a model that is almost as good as the original working model. Spectra and kinetics for this model obtained after some adjustments of all the site energies (see the resulting set E47 in Table S2) are shown in Figs. S3 and S4. In this model the PEB_{82D} pigment is the lowest one, i.e. lower than the other peripheral sites, DBV_A and DBV_B. In addition, its population growth during the first 5 ps is slower than for DBV's. As a result the dynamics of the site populations is similar to the working model, but the slow redistribution between the red sites in the time scale of 50 ps is more pronounced (Figs. S5 and S6).

In the energy transfer scheme (Fig. S7) we see relatively slow population of PEB_{82D} via $PEB_{50/61D} \rightarrow PEB_{50/61C} \rightarrow DBV_B \rightarrow PEB_{82D}$ pathway. In the working model population of PEB_{82C} (occupying the same spectral position as PEB_{82D} in alternative model) occurs faster via more direct and short chain, i.e. $PEB_{50/61D} \rightarrow PEB_{50/61C} \rightarrow PEB_{82C}$. (The complexity of the E47 model probably cannot give a preference to more elegant working model, but the latter also gives a better fit of the data).

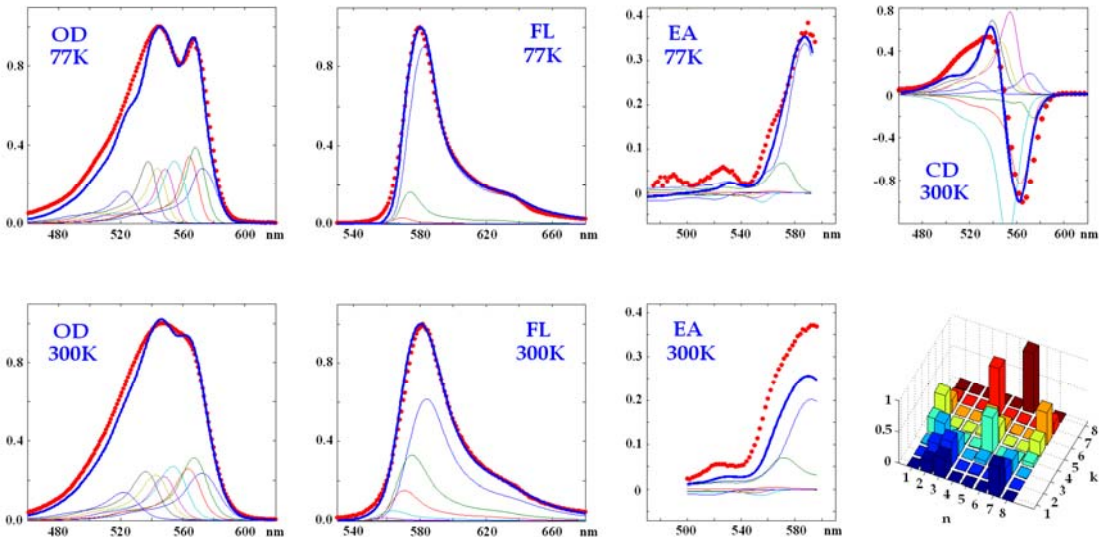

Fig. S3. Fit of the steady-state spectra with the model E47. This is the same fit as shown in Fig. 2, but now with the model E47 instead of model E.

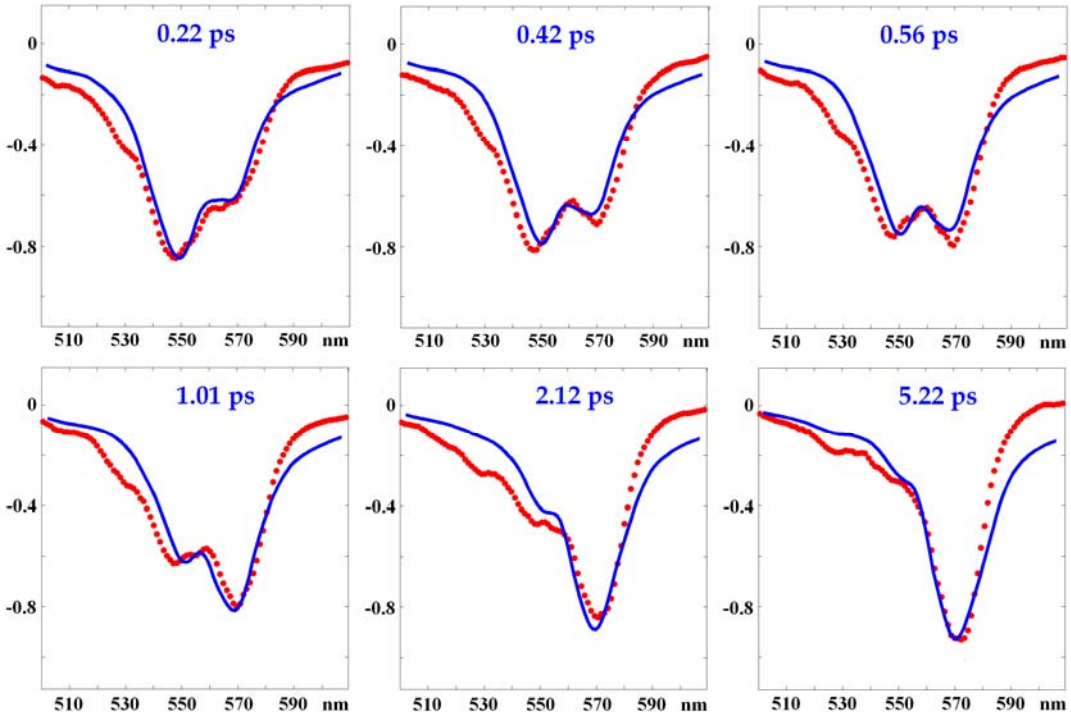

Fig. S4. Fitting of the 77K TA spectra upon 505 nm excitation at pump-probe delays of 0.22, 0.42, 0.56, 1.01, 2.12, and 5.22 ps with the model E47. This is the same fit as in Fig. 3, but with the model E47 instead of model E.

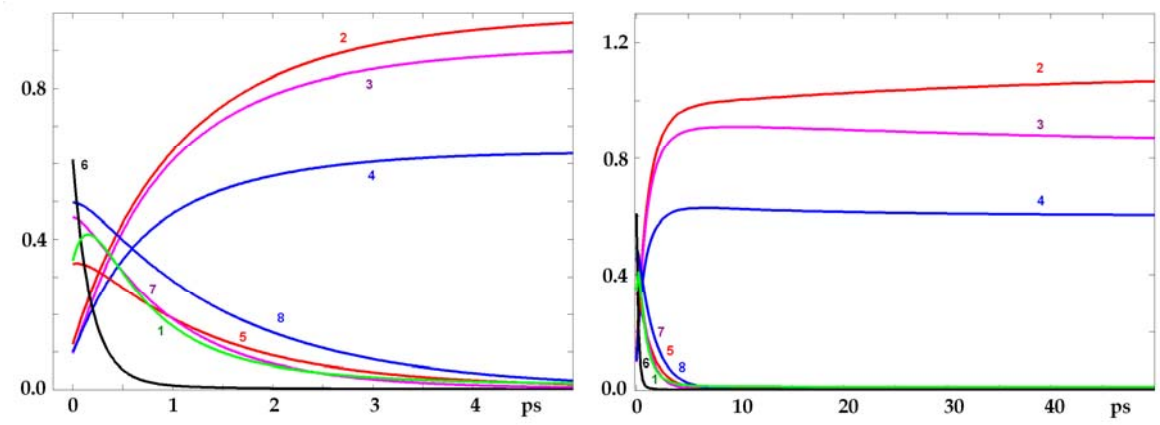

Fig. S5. Time-dependent site populations (arbitrary units) upon 505 nm excitation calculated with the working model E. Time delays are 0-5 ps (left) and 0-50 ps (right). The dynamics is averaged over disorder.Order of the sites (numbered from 1 to 8) is the same as in Table 1, i.e.

1	2	3	4	5	6	7	8
$PEB_{50/61C}$	DBV_A	DBV_B	PEB_{82C}	PEB_{158C}	$PEB_{50/61D}$	PEB_{82D}	PEB_{158D}

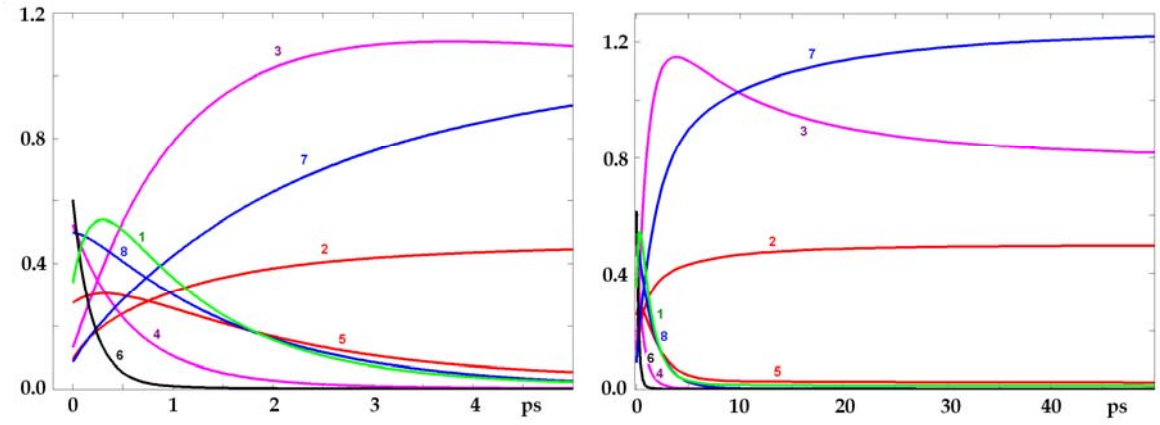

Fig. S6. The same as in Fig. S5, but now for the model E47. Colors are the same as in Fig. S5, but now the rising blue curve is 7 instead of 4 in Fig. S5, and decaying magenta is 4 instead of 7 in Fig. S5.

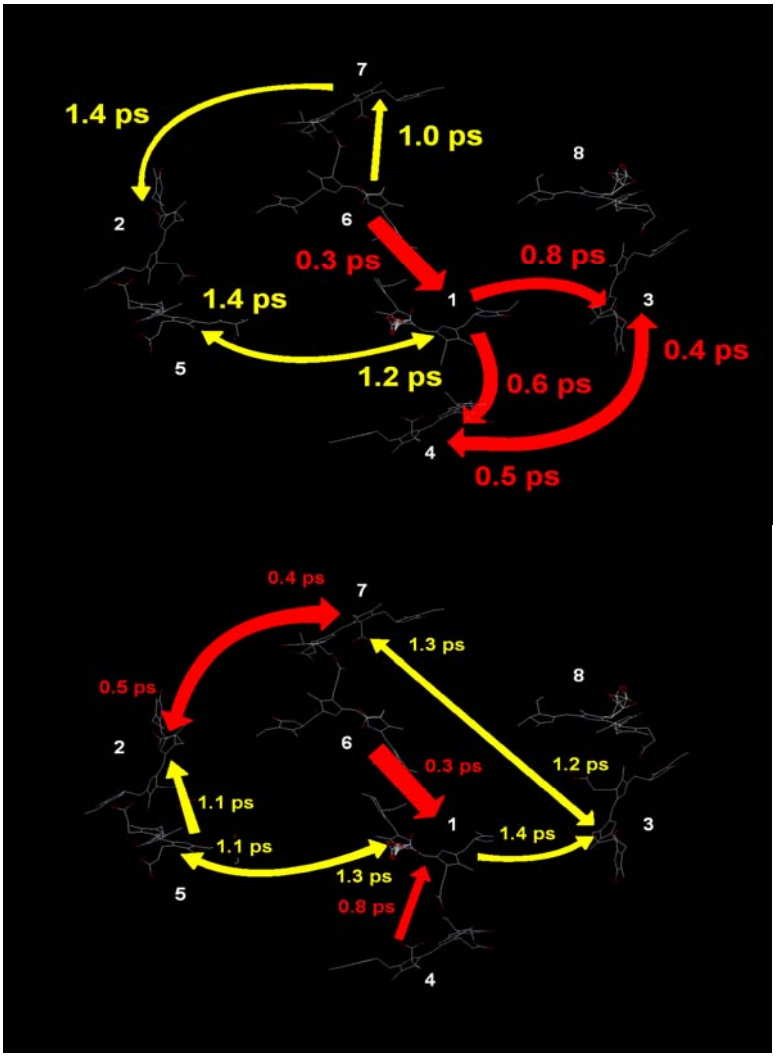

Fig. S7. Time constants for energy transfer in the site representation (with averaging over disorder) for the working model E (top frame) and model E47 (bottom frame). Transfer pathways with the time constant less than 1 ps (red arrows) and less than 1.5 ps (yellow arrows) are shown. The data in the top frame is the same as in Fig. 6.

Table S3. Time constants of energy transfer (ps) from the n-th site to the n'-th one (averaged over disorder)* for Models E and E47. Time constants in the 0-1 ps, 1-2 ps, 2-3 ps, and 3-4 ps ranges are shown by red, orange, green, and cyan, respectively. Negative values on the diagonal correspond to lifetimes of the corresponding site (sum of all the off diagonal rates).

	n=1	2	3	4	5	6	7	8
	Model E							
n'=1	-0.2484	9.9117	2.8041	2.0316	1.1741	0.3500	2.9763	7.5860
n'=2	3.6458	-0.8040	1.5140	1.5964	1.9084	2.0778	1.3836	14.7228
n'=3	0.7915	1.6429	-0.3219	0.4194	7.3619	6.6663	9.1499	2.3926
n'=4	0.6494	2.0234	0.4856	-0.2826	4.9073	3.1776	11.0089	8.0530
n'=5	1.3718	38.6635	64.5138	43.6136	-0.5034	1.8961	5.5744	5.7880
n'=6	67.1203	621.5971	386.4719	279.3667	88.5042	-0.1722	5.9795	21.1706
n'=7	7.1386	163.2658	240.6102	334.9471	8.4718	1.0958	-0.5221	3.5115
n'=8	15.4093	156.0086	126.6351	176.0643	7.0431	1.7774	3.2274	-0.8021
	Model E47							
n'=1	-0.3776	16.3530	10.7934	0.8125	1.2610	0.3192	26.0318	2.7576
n'=2	5.3751	-0.2778	1.6623	13.3874	1.1460	1.6167	0.5028	25.0276
n'=3	1.3977	1.3941	-0.6349	1.5004	5.1131	9.1657	1.2137	1.8693
n'=4	3.2988	322.9241	126.5882	-0.3938	19.2245	3.8945	512.7064	8.8232
n'=5	1.1285	2.6512	12.2308	3.6355	-0.4199	2.3258	7.6693	8.5741
n'=6	34.4301	415.6292	549.2580	17.0558	91.5888	-0.1787	603.1274	21.5938
n'=7	4.4525	0.4113	1.2973	14.9234	2.6570	1.9021	-0.3346	16.5614
n'=8	3.2901	155.7544	53.8040	6.0036	12.3442	1.9067	266.3909	-0.7848

*In principle the transfer rate between any pair of pigments can be calculated by averaging over disorder as $R_{n'n'nn}=(c_{n'}^{k'})^2 R_{k'k'kk} (c_n^k)^2$. Here the rate of k→k' transfer (Eq. S14) is combined with the participation of the pigments n and n' in the corresponding states, thus giving the rate of n→n' transfer. Such a formal definition is only possible in case the exciton states are almost localized, i.e. when the amplitudes c_n^k are always close to unity for all realizations of the disorder. Using this definition it is possible to calculate the site-to site rates with averaging over disorder, because the c_n^k factor always fixes the exciton level where the n-th pigment is participating (although the ordering of exciton states can be different for different realizations of the disorder). Here we show the time constants of energy transfer from the n-th site to the n'-th one (calculated as the $R_{n'n'nn}^{-1}$ values averaged over disorder) for models E and E47.

Different order of the lowest-energy states (Comparing model E42 with the working model E)

Finally, we have tried a different order of energies for the three lowest pigments (DBV_A, DBV_B, and PEB_{82C}). We have found a good configuration (model E42 in Table S2), where PEB_{82C} is lower in energy than the two DBV's (in contrast to the working model, where PEB_{82C} is higher).

For this model the steady-state spectra are acceptable (Fig. S8), and the TA kinetics are almost the same as for model E (data not shown). The energy transfer rates are not much different to those in the working model (see Table S4). We conclude that variation in the order of the site energies within the 567 nm sub-band does not produce any significant changes in the model of the complex. This is not surprising, bearing in mind that these sites have very close transition energies.

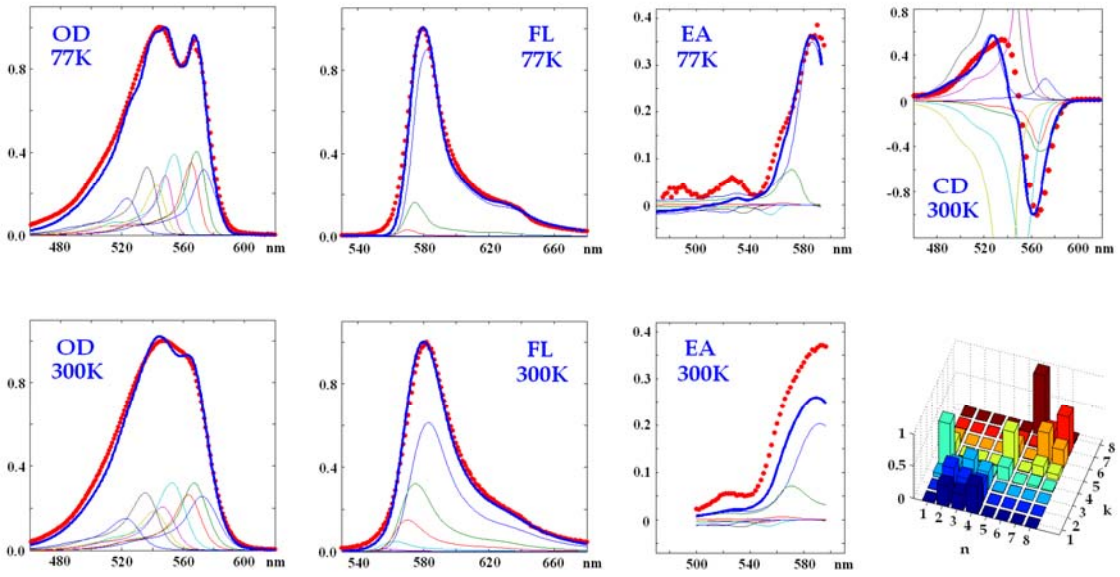

Fig. S8. Fit of the steady-state spectra for model E42. This is the same fit as shown in Fig. 2, but now with the model E42 instead of model E.

Table S4. Time constants of energy transfer (ps) from the n-th site to the n'-th one (averaged over disorder)* for Models E and E42. Time constants in the 0-1 ps, 1-2 ps, 2-3 ps, and 3-4 ps ranges are shown by red, orange, green, and cyan, respectively. Negative values on the diagonal correspond to lifetimes of the corresponding site.

	n=1	2	3	4	5	6	7	8
	Model E							
n'=1	-0.2484	9.9117	2.8041	2.0316	1.1741	0.3500	2.9763	7.5860
n'=2	3.6458	-0.8040	1.5140	1.5964	1.9084	2.0778	1.3836	14.7228
n'=3	0.7915	1.6429	-0.3219	0.4194	7.3619	6.6663	9.1499	2.3926
n'=4	0.6494	2.0234	0.4856	-0.2826	4.9073	3.1776	11.0089	8.0530
n'=5	1.3718	38.6635	64.5138	43.6136	-0.5034	1.8961	5.5744	5.7880
n'=6	67.1203	621.5971	386.4719	279.3667	88.5042	-0.1722	5.9795	21.1706
n'=7	7.1386	163.2658	240.6102	334.9471	8.4718	1.0958	-0.5221	3.5115
n'=8	15.4093	156.0086	126.6351	176.0643	7.0431	1.7774	3.2274	-0.8021
	Model E42							
n'=1	-0.2560	18.9973	2.9372	3.0692	1.0309	0.3442	2.9471	7.0787
n'=2	3.9844	-0.6951	1.4125	1.3082	1.7589	2.1835	1.2822	14.5895
n'=3	0.7094	1.5909	-0.2765	0.4524	5.5315	5.3822	7.7108	2.6054
n'=4	0.8633	1.4308	0.3969	-0.3006	6.4841	4.0151	11.0146	9.0161
n'=5	1.2043	20.6366	25.8719	58.2122	-0.4548	1.8691	4.1912	6.9467
n'=6	67.4358	749.3002	380.6358	391.3014	83.4306	-0.1728	10.1032	6.8486
n'=7	5.0529	160.9660	221.3673	294.8941	4.9430	1.1420	-0.4974	2.8360
n'=8	22.6063	382.4596	314.6064	343.0015	9.0068	1.7329	3.0014	-0.7423

*The time constants are calculated as the $R_{n'n'nn}^{-1}$ values averaged over disorder.

References

Mukamel, S. 1995. Principles of Nonlinear Optical Spectroscopy. Oxford University Press, New York.

Doust, A. B., C. N. J. Marai, S. J. Harrop, K. E. Wilk, P. M. G. Curmi, and G. D. Scholes. 2004. Developing a structure-function model for the cryptophyte phycoerythrin 545 using ultrahigh resolution crystallography and ultrafast laser spectroscopy. J. Mol. Biol. 344:135-153.

Novoderezhkin, V. I. M. Wendling, and R. van Grondelle. 2003. Intra- and interband transfers in the B800–B850 antenna of *Rhodospirillum molischianum*: Redfield theory modeling of polarized pump-probe kinetics. J. Phys. Chem. B. 107:11534–11548.

Novoderezhkin, V. I., M. A. Palacios, H. van Amerongen, and R. van Grondelle. 2004. Energy-transfer dynamics in the LHCII complex of higher plants: modified Redfield approach. J. Phys. Chem. B. 108: 10363-10375.

Novoderezhkin, V. I., E. G. Andrizhiyevskaya, J. P. Dekker, and R. van Grondelle. 2005. Pathways and timescales of primary charge separation in the photosystem II reaction center as revealed by a simultaneous fit of time-resolved fluorescence and transient absorption. Biophys. J. 89:1464-1481.

Zhang, W. M., T. Meier, V. Chernyak, and S. Mukamel. 1998. Exciton-migration and three-pulse femtosecond optical spectroscopies of photosynthetic antenna complexes. J. Chem. Phys. 108:7763-7774.